Ann. Geophys., 28, 1289–1297, 2010
www.ann-geophys.net/28/1289/2010/
doi:10.5194/angeo-28-1289-2010

Annales Geophysicae

Simulation of mode conversion process from upper-hybrid waves to LO-mode waves in the vicinity of the plasmapause

M. J. Kalaee[1], **Y. Katoh**[1], **A. Kumamoto**[2], **T. Ono**[1], **and Y. Nishimura**[3]

[1]Department of Geophysics, Graduate School of Science, Tohoku University, Sendai, Japan
[2]Planetary plasma and Atmospheric Research Center, Graduate School of Science, Tohoku University, Sendai, Japan
[3]Solar-Terrestrial Environment Laboratory, Nagoya University, Nagoya, Japan

Received: 21 August 2009 – Revised: 21 May 2010 – Accepted: 26 May 2010 – Published: 14 June 2010

Abstract. In order to clarify the role of the mode conversion process in the generation mechanism of LO-mode waves in the equatorial region of the plasmasphere, we have investigated the linear mode conversion process among upper-hybrid-resonance (UHR)-mode, Z-mode and LO-mode waves by a numerical simulation solving Maxwell's equations and the equation of motion of a cold electron fluid. The wave coupling process occurring in the cold magnetized plasma are examined in detail. In order to give a realistic initial plasma condition in the numerical experiments, we use initial parameters inferred from observation data obtained around the generation region of LO-mode waves obtained by the Akebono satellite. A density gradient is estimated from the observed UHR frequency, and wave normal angles are estimated from the dispersion relation of cold plasma by comparing observed wave electric fields. Then, we perform numerical experiments of mode conversion processes using the density gradient of background plasma and the wave normal angle of incident upper hybrid mode waves determined from the observation results. We found that the characteristics of reproduced LO-mode waves in each simulation run are consistent with observations.

Keywords. Magnetospheric physics (Plasma waves and instabilities)

Correspondence to: M. J. Kalaee
(j_kalaee2000@yahoo.com)

1 Introduction

The mode conversion of upper-hybrid-resonance (UHR) mode waves ($\omega_p < \omega \leq \omega_{uh}$) to Z-mode ($\omega_z < \omega \leq \omega_p$) and LO-mode ($\omega \geq \omega_p$) waves has been investigated for the purpose of understanding the origin of planetary radio emissions, where ω is the wave frequency, ω_p is the electron plasma frequency, ω_{uh} is the UHR frequency, and ω_z is the cutoff frequency of Z-mode waves. The double mode conversion theory proposed by Oya (1971) has been applied to generation processes of Jovian decametric radiation (Oya, 1974) and auroral kilometric radiation (AKR) (Benson, 1975). The mode conversion mechanism consists of three processes. In the first process, field–aligned precipitating beams and/or anisotropies of velocity distributions of energetic electrons excite electrostatic electron cyclotron harmonic waves. These electrostatic waves propagate toward lower plasma density regions until these waves encounter the electrostatic resonance frequency, as has been experimentally identified by Warren and Hagg (1968). In the second process, the electrostatic electron cyclotron harmonic waves are converted to UHR-mode waves, reflected back toward higher plasma densities. These waves are further converted to Z-mode radio waves toward the high density region. In the third process, the Z-mode waves propagate into the plasma frequency layer of $\omega = \omega_{pe}$, where these waves have a chance to convert into ordinary (LO-mode) waves. There are some variations of conversion mechanisms generating LO-mode waves from planetary plasma. A typical example is a generation process of non-thermal continuum (NTC) radiation, which is one of the common radio emissions in planetary magnetospheres. The fundamental characteristics of observed continuum radiation have been explained by the

Published by Copernicus Publications on behalf of the European Geosciences Union.

linear mode conversion theory (LMCT) (Jones, 1976, 1977, 1980; Lembege and Jones, 1982). In LMCT, electrostatic waves are generated by unstable electron distributions, and then transformed into the Z-mode radiation during the wave propagation. When the Z-mode waves encounter the layer with $\omega = \omega_{\rm pe}$ or the radio window, a part of the wave energy is converted into the LO-mode waves with the wave frequency equal to the local plasma frequency $\omega_{\rm pe}$ at the radio window and escape to free space with a beaming angle of $\alpha_{\rm LMCT} = \pm\tan^{-1}\sqrt{\omega_{\rm ce}/\omega_{\rm pe}}$ with respect to the magnetic equator, where $\omega_{ce}$is the electron cyclotron frequency (Jones et al., 1987). Previous observations and theories have been reviewed in detail by Hashimoto et al. (2005, 2006). Grimald et al. (2007) investigated a quantitative test of Jones NTC beaming theory by using CLUSTER constellation. Their studies have demonstrated the difficulty of validating NTC linear generation mechanisms using global beaming properties alone. There arises difficulty in theoretical treatments in a case that the spatial size of inhomogeneity is of the order of the wavelength of LO-mode waves, where the WKB approximation is invalid. The simulation studies have also pointed out that efficient LO-mode wave generation is expected in the case that the spatial scale of the density gradient is the order of wavelength (Katoh and Iizima, 2006; Kalaee et al., 2009).

In order to clarify the role of the mode conversion process in the generation mechanism of LO-mode waves in the plasmasphere, a numerical experiment can be a highly useful tool for a guiding theory. We investigate the linear mode conversion process among UHR-mode, Z-mode and LO-mode waves by a computer simulation solving Maxwell's equations and the equation of motion of a cold electron fluid. In order to give a realistic initial plasma condition in the numerical experiments, we used the observation data obtained by the Akebono satellite in the region close to the plasmapause. Three typical examples of the Akebono observation are compared with the simulation results. We estimate the density gradient of background plasma from the variation of the UHR frequency observed by the plasma wave and sounder (PWS) instrument onboard the Akebono satellite, and we analyze the incident wave normal angle by comparing observed electric field components with the dispersion relation of cold plasma. Using the initial condition inferred from the observation data, we performed the numerical experiments corresponding to each observed event. Based on the simulation results, we discuss dependence of conversion efficiency on the direction of propagation vectors. We study the wave normal angle, electric field components and the beaming angle of reproduced LO-mode waves in the numerical experiments for a comparison with the observation. In Sect. 2, we describe the instrumentation and data set used in the present study. Three typical events observed by the Akebono satellite at the site of mode conversion are described in Sect. 3. The simulation model and results of the numerical experiments are described in Sect. 4. Discussions of the characteristics of mode conversion processes reproduced in the simulation results are given in Sect. 5. Conclusions are mentioned in Sect. 6.

2 Instrumentation and data set

The Akebono satellite is in a quasi-polar orbit with initial perigee and apogee of 1.04 and 2.6 $R_{\rm E}$, where $\rm R_E$ is the radius of the Earth, and its orbital period is 210 min. The spacecraft spin axis is oriented to the sun and the spacecraft spin period is 8 s. The PWS experiments on board the Akebono satellite was designed to operate in both an active mode and a passive mode which are detailed by Oya et al. (1990). The passive measurements are used in this study. The signals from the two orthogonal electric field antennas are simultaneously fed to the PWS receiver. The two X and Y antennas have a tip-to-tip length of 60 m perpendicular to the sun direction. The both $E_{\rm x}$ and $E_{\rm y}$ intensity from the dipole antennas are used in the present study. Three typical observation events at the site of mode conversion analyzed in this study are found during the period from October 1990 to March 1992, as shown in the next section.

3 Observations

In order to clarify the role of the mode conversion process in the generation mechanism of LO-mode waves in the plasmasphere, we analyze three typical observation events at the site of the mode conversion. The spectrograms of each event are shown in Fig. 1a–c.

Event 1 is found during the period from 22:30 to 23:00 UT on 21 March 1991. In the Event 1, the UHR frequency is observed between 380 and 120 kHz as shown in Fig. 1a. This result clearly shows an existence of large inhomogeneity from 22:37 to 22:44 UT. A narrow band of LO-mode waves is observed around the 22:43 UT in the frequency 205 kHz and with the cyclotron frequency, $f_{\rm c} = 91.8$ kHz. The power of two components of electric field, $E_{\rm x}$ and $E_{\rm y}$, are -153 dBV/m Hz$^{1/2}$ and -148.9 dBV/m Hz$^{1/2}$, respectively, for UHR-waves with a frequency $\sim$205 kHz at 22:42:37 UT and are -157.5 dBV/m Hz$^{1/2}$ and -157.8 dBV/m Hz$^{1/2}$ for LO-waves with the same frequency at 22:43:00 UT.

Event 2 is found during the period from 12:07 to 12:30 UT on 22 March 1991. In this event, the UHR frequency varies from 390 to 125 kHz as shown in Fig. 1b. Large inhomogeneity of the background plasma could be expected from 12:20:42 to 12:24:00 UT. We also find that a narrow band of LO-mode waves is observed after 12:23 UT. Powers of $E_{\rm x}$ and $E_{\rm y}$, are -147.3 dBV/m Hz$^{1/2}$ and -150 dBV/m Hz$^{1/2}$, respectively, for UHR-waves with a frequency of $\sim$143 kHz at 12:22:48 UT and are -155 dBV/m Hz$^{1/2}$ and -154 dBV/m Hz$^{1/2}$ for LO-waves

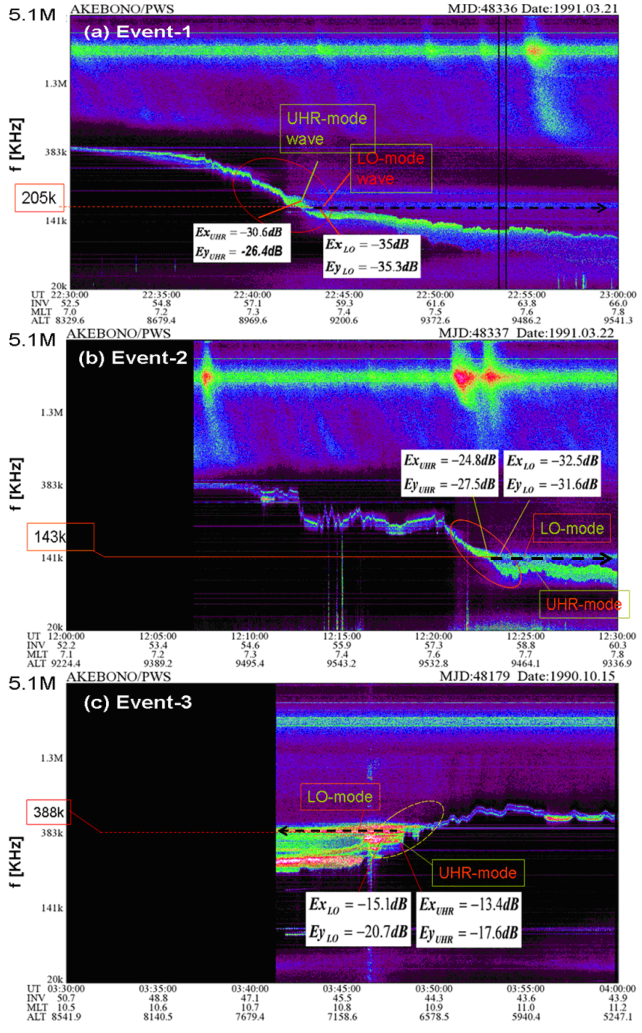

Fig. 1. Akebono satellite observation of plasma waves around the plasmapause. The figures indicate three examples of the dynamic spectrum, that LO-mode can be generated by mode conversion process. We focus on the area inside the circles shown in each panel.

with the same frequency at 12:23:30 UT, and with the cyclotron frequency $f_c = 69$ kHz.

Event 3 is observed during a period from 03:41 to 04:00 UT on 15 October 1990. As shown in Fig. 1c, the UHR frequency varies from 260 to 600 kHz. We find a steep density gradient between 03:48:05 and 03:48:30 UT and a band of LO-mode waves until 03:48:24 UT. The power of E_x and E_y, are -135.9 dBV/m Hz$^{1/2}$ and -140 dBV/m Hz$^{1/2}$, respectively, for UHR-waves with a frequency of ∼388 kHz at 03:48:08 UT and -137.6 and -143.2 dB for LO-waves with the same frequency at 03:47:00 UT, and with the cyclotron frequency $f_c = 109$ kHz. The satellite position corresponds to the plasmasphere in each event as shown in Fig. 2.

We found in these three events that a band of LO-mode waves has been observed around the density gradient, while the observed wave amplitudes of LO-mode waves are similar to those of UHR waves simultaneously observed by the Akebono satellite. Here we assume this emission to be emitted in LO-mode from the locally observed UHR waves through the mode conversion process in the inhomogeneous plasma. In the next section, so as to verify this hypothesis, we conduct numerical experiments using plasma parameters observed by the Akebono satellite.

4 Simulation model

We study the wave coupling process among UHR-mode, Z-mode and LO-mode waves by using a spatially two-dimensional electron fluid model (Katoh, 2003; Katoh and Iizima, 2006; Kalaee et al., 2009). The basic equations are given as follows;

$$\frac{\partial V}{\partial t} = -(V\cdot\nabla)V + \frac{q}{Nm}(\boldsymbol{E} + V\times\boldsymbol{B}) \tag{1}$$

$$\frac{\partial N}{\partial t} = -\nabla\cdot(NV) \tag{2}$$

$$\frac{\partial \boldsymbol{B}}{\partial t} = -\nabla\times\boldsymbol{E} \tag{3}$$

$$\frac{\partial \boldsymbol{E}}{\partial t} = \frac{1}{\varepsilon_0\mu_0}\nabla\times\boldsymbol{B} - \frac{1}{\varepsilon_0}J \tag{4}$$

where $\boldsymbol{E}$ is electric field, $\boldsymbol{B}$ is magnetic field, J is current density, V and N are the velocity and number density of an electron fluid. The equation of motion and the continuity equation coupled with Maxwell's equations are solved by using the two-step Lax-Wendroff scheme. Each physical value is normalized to a dimensionless quantity; time is normalized by electron cyclotron frequency ω_c, the velocity and length are normalized by the speed of light c and c/ω_c, respectively. We use the grid spacing ΔX and ΔY of $1\times10^{-2}c/\omega_c$ and a time step Δt of $7.5\times10^{-3}\omega_c^{-1}$.

Figure 3 schematically indicates the two-dimensional simulation box used in the present study. The external magnetic field $\boldsymbol{B}_0$ is assumed to lie in the X-Y plane. We assume that the simulation system is immersed in a cold plasma fluid. The simulation box consists of three regions: homogeneous regions with plasma frequencies of ω_{pA} (Region-A) and ω_{pB} (Region-B) smoothly connected by an inhomogeneous region. We generate plasma waves by oscillating X- and Z-components of the electric field in the wave generation region, while the wave vector $\boldsymbol{k}$ of generated waves is introduced to be aligned with the X-axis making an oblique propagation to the external magnetic field. To avoid any effects due to reflected waves from the boundary of the simulation box, we set damping regions at the edges of the simulation system so as to suppress the reflection of outgoing waves.

The density gradient was set perpendicular to $\boldsymbol{B}_0$. For each observed event described in the previous section, we

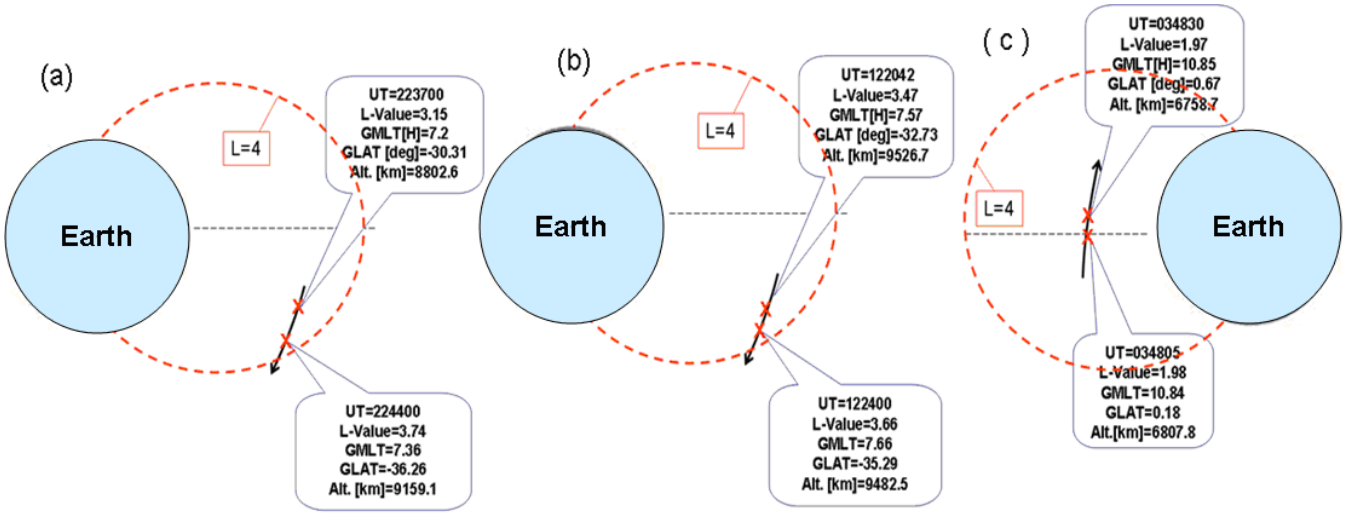

Fig. 2. Schematic illustration of satellite path for three Events 1, 2 and 3, respectively.

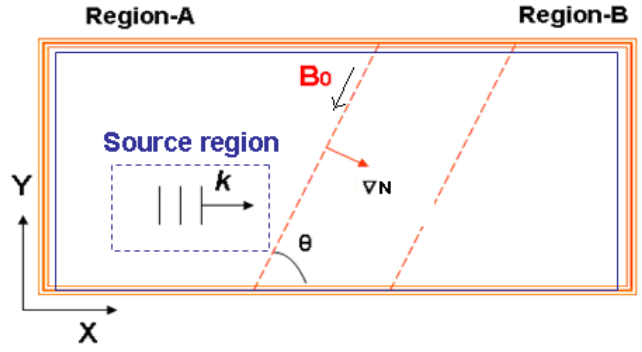

Fig. 3. Schematic illustration of the simulation system. We assume homogenous regions with plasma frequencies of ω_{pA} (Region-A) and ω_{pB}(Region-B) smoothly connected by an inhomogeneous region where the density gradient ∇N is assumed.

obtained the angle between the density gradient and the magnetic field by using the displacement vector of the spacecraft, magnetic field vector, temperature and number density of the background plasma. During geomagnetic storms, plasma around the plasmapause flows out to the magnetosphere and is filled again from the ionosphere. Figure 4a–b shows the magnetic activity for each event that indicate there are not any magnetic storm at the date of each event.

By applying the ISEE/Whistler model (Carpenter and Anderson, 1992) and based on the Akebono data the angle between the magnetic field and the density gradient is estimated, for example for Event-1 is given by:

$$|\nabla N| = 4930/m^4$$

$$\nabla N_{||} = 4.93/m^4$$

$$\alpha = \cos^{-1}\frac{|\nabla N_{||}|}{|\nabla N|} \approx 89.9^\circ$$

Where $|\nabla N|$ and $|\nabla N_{||}|$ are the magnitude of density gradient observed by the Akebono satellite and the magnitude of density gradient component, parallel to the magnetic field respectively, α is an angle between the density gradient and $\boldsymbol{B}_0$. We assume, the density gradient is perpendicular to the magnetic field, ($\nabla N \sim \nabla_{\perp} N$).

In Fig. 5a–c, we show profiles of the plasma and UHR frequencies as a function of time observed in the Event 1 (from 22:41 to 22:43 UT on 21 March 1991), Event 2 (from 12:18 to 12:30 UT on 22 March 1991) and Event 3 (from 03:41 to 03:50 UT on 15 October 1990). Based on the result of observations, we give the plasma frequencies in Regions A and B in the simulation system. Namely, in the Run-1 of the simulation corresponding to the Event 1, we assume $\omega_{pA}/\omega_{ce} = 2.2$($f_{pA}$=201.9 kHz) and $\omega_{pB}/\omega_{ce} = 2.76$($f_{pB}$=252.1 kHz). In the Run-2 corresponding to the Event 2, we assume $\omega_{pA}/\omega_{ce} = 2.029$($f_{pA}$=140 kHz) and $\omega_{pB}/\omega_{ce} = 2.73$ (f_{pB}=188.8 kHz). We assume in the Run-3 corresponding to the Event 3 that $\omega_{pA}/\omega_{ce} = 3.532$($f_{pA}$=385 kHz) and $\omega_{pB}/\omega_{ce} = 4.266$ (f_{pB}=452 kHz).

In order to estimate the wave normal angle of the incident UHR-mode waves, we compared the observed wave electric field components with the dispersion relation of cold plasma. First, we examined three components of the wave electric field from the dispersion relation for all wave normal angles, and then we converted them into the spacecraft coordinate. By comparing the projected wave electric field components with two components of the observed wave electric fields, we determined the wave normal angles of observed waves when the observed E_x/E_y ratio was almost equal to the E_x/E_y ratio

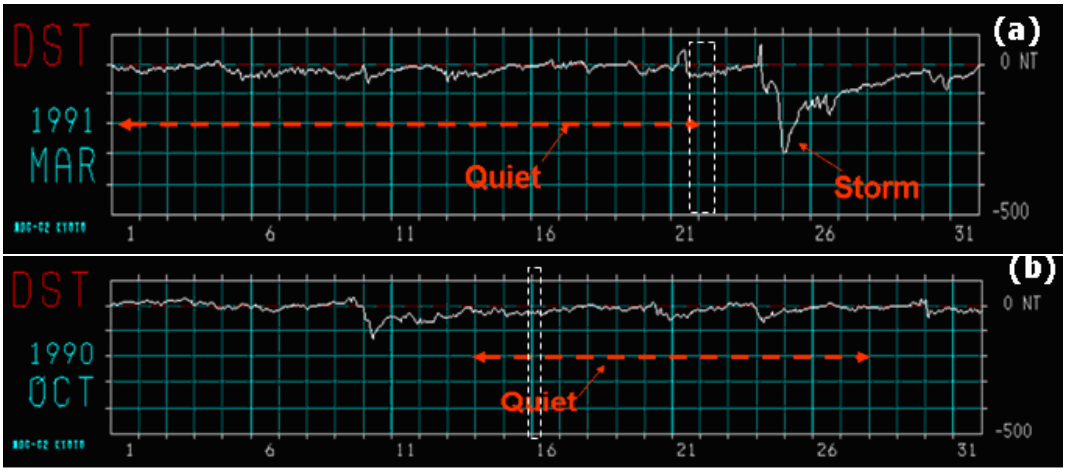

Fig. 4. The magnetic activity during the observation period of each event that these are not severely disturbed time, but already disturbed in some periods. The dash rectangle shows the date for each event. **(a)** 21 and 22 March 1991. **(b)** 5 October 1990. (This data is provided by World Data Center (WDC) Kyoto.)

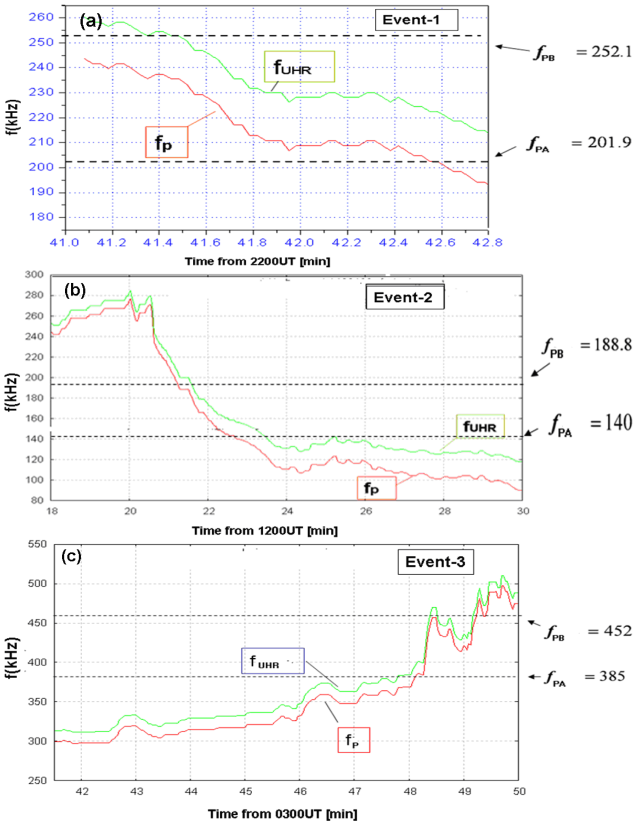

Fig. 5. Profiles of plasma and UHR frequencies vs UT for three events.

derived from the dispersion relation. The steps of the wave normal angles estimation as follows:

1. Two electric field components E_x and E_y were obtained from observation in the satellite coordinate (Fig. 6a).

2. Three components of electric field (E'_x, Ey', E'_z) estimated for a wave normal angle (θ') by using the dispersion relation in the coordinate where the Z′-axis is along $\boldsymbol{B}_0$ (Fig. 6b); Then these components ware converted in the equatorial coordinates by using the direction $\boldsymbol{B}_0$ in the equatorial coordinates. Finally by using the direction of X and Y antennas in equatorial coordinate, three components ware estimated in the satellite coordinates.

3. By changing the wave normal angle in the prime coordinate and repeating the process, the wave normal angle whose the ratio of E_x and E_y is closed to observation was chosen.

The estimated wave normal angles are summarized in Table 2.

For an example of the simulation results, we show the result of the Run-2 in Fig. 7. A part of the incident UHR-mode waves are transmitted into Z-mode waves over the location where $\omega = \omega_{pe}$ in the inhomogeneous medium, while the other part of wave energy are reflected toward the Region-A as both UHR-mode and LO-mode waves. The transmitted waves cannot propagate further into the Region-B because the wave frequency is lower than the cutoff frequency of Z-mode waves in the Region-B. Therefore the transmitted Z-mode waves are reflected when they encounter the local cutoff frequency of Z-mode waves and again encounter to the layer with $\omega = \omega_{pe}$, resulting in the mode conversion

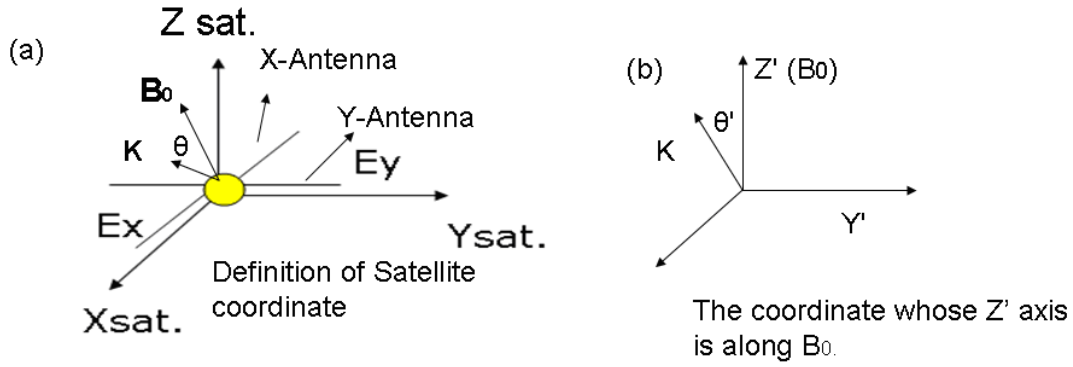

Fig. 6. Schematic illustration of **(a)** the definition of satellite coordinate and **(b)** the coordinate whose Z′-axis is along $\boldsymbol{B}_0$.

Table 1. Parameters used in this study; wave normal angle, cyclotron frequency, incident wave frequency and plasma frequency, UHR-frequency and Z-cutoff in Region A and B (All of frequencies are in kHz).

	Wave normal angle ($\theta°$)	f_{ce}	$f_{Inc.}$	wavelength $\lambda\left[c\Omega^{-1}\right]$	f_{p-A}	f_{UHR-A}	$f_{Z-cutoff-A}$	f_{p_B}	f_{UHR_B}	$f_{Z\_cutoff\_B}$	Validity of WKB $\Delta\lambda/\lambda$
Event-1	55	91.8	205	0.396	201.9	221.79	161.15	252.1	268.29	210.34	0.1
Event-2	61.8	69	143	0.426	140	156.08	109.68	188.8	201	157.43	0.75
Event-3	71	109	388	0.248	385	400.0	334.24	452	465	400.7	0.9

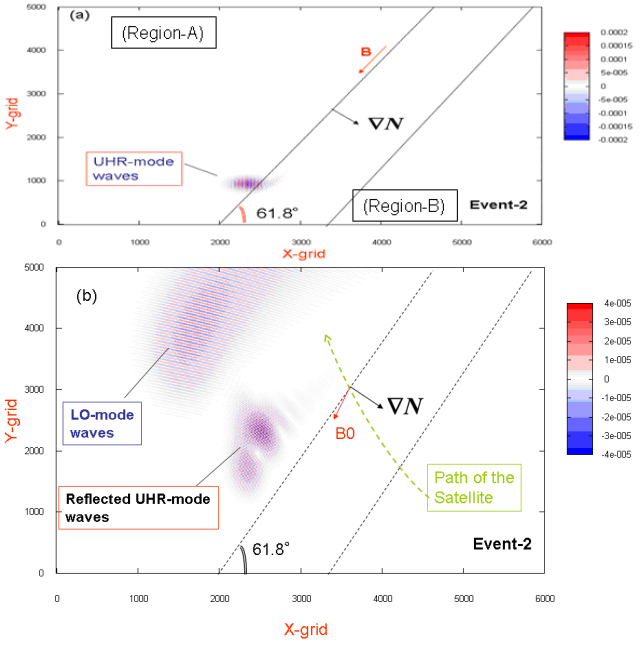

Fig. 7. Spatial distribution of the E_x component of the electric field in the simulation system at **(a)** t=52.5ω_c^{-1} and **(b)** t=172ω_c^{-1} in Event-2.

from Z-mode to LO-mode waves. We found that the simulation results clearly reproduced the generation of LO-mode waves through the mode conversion process. In order to examine the coupling properties between UHR-mode and LO-mode waves, we performed FFT analyses on the wave electric field to obtain the spatial distribution of frequency and wave number spectra. In each simulation run, we confirmed that the polarization of incident waves corresponds to that of UHR waves. Figure. 7a and b, respectively, indicates the spatial distributions of the X component of the electric field at t=52.5ω_c^{-1} and t=172ω_c^{-1}, corresponding to the time periods before and after the mode conversion process occurred around t=60ω_c^{-1}. By analyzing the polarization of LO-mode waves ($E_x/E_z \approx 0.98$ and $k_x \approx 0.43$, $k_y \approx 1.12$), we estimated the wave normal angle of the converted LO-mode is nearly 7.2 degrees apart from the ambient magnetic field in the Region-A. We found that the wave normal angle of reproduced LO-mode waves in the simulation result of the Run-2 is consistent with the wave normal angle of observed LO-mode waves in the Event 2. Such consistency between the simulation result and the observation is also found in each simulation run. We summarize the simulation results in Table 2.

Table 2. Summary of simulation results. The left column shows a comparison with the dispersion relation for both observation and simulation for incident and LO-mode waves. The right column shows an amplitude comparison between simulation results and observations.

		Comparison with dispersion relation				Amplitude comparison			
		Wave normal angle (θ°) in Region-A	$(E_x/E_y)_{Dis.}$	$(E_x/E_y)_{Obs.}$	$(E_x/E_y)_{Sim.}$	$(E_{x\,Lo}/E_{x\,UHR})_{Obs.}$	$(E_{x\,Lo}/E_{x\,UHR})_{Sim.}$	$(E_{y\,Lo}/E_{y\,UHR})_{Obs.}$	$(E_{y\,Lo}/E_{y\,UHR})_{Sim.}$
Event-1	UHR	55	0.65	0.63	0.64	0.60	0.62	0.36	0.38
	LO	5.5	1.036	1.035	1.034				
Event-2	UHR	61.8	1.36	1.36	1.37	0.42	0.41	0.62	0.61
	LO	7.2	0.9	0.9	0.89				
Event-3	UHR	71	1.63	1.62	1.64	0.82	0.83	0.69	0.67
	LO	10	1.91	1.9	1.92				

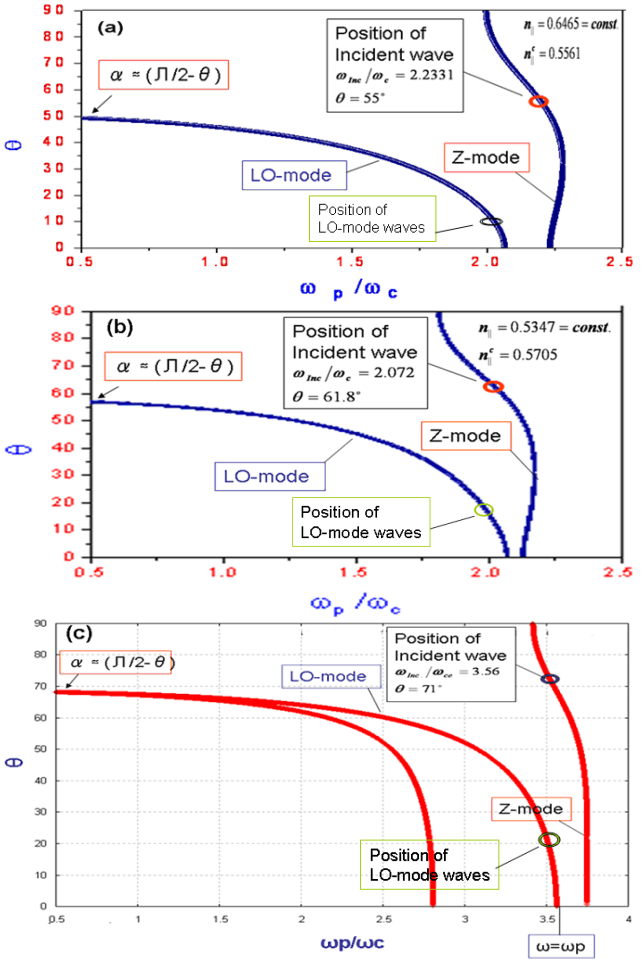

Fig. 8. Variation of wave normal angles vs. ω_p/ω_{ce} under a condition that $n_{||}$ is constant, that slightly different with critical values, two branches of Z-mode and LO-mode waves is disconnected. Each panel corresponds to the settings used in Runs A, B and C.

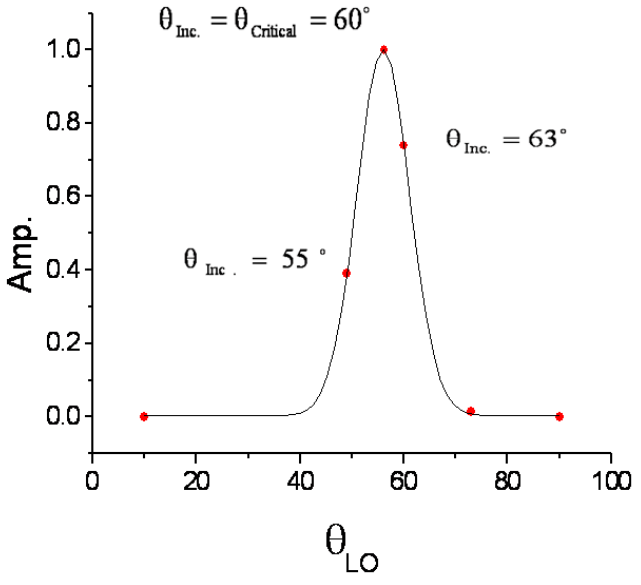

Fig. 9. The relative wave amplitude profile as a function of estimated wave normal angle of LO-mode wave escaping to free space for Event-1 with different incident wave normal angle ($\theta_{Inc.}$).

5 Discussion

According to the theory in the cold plasma (Jones, 1980), for the "critical value" of the refractive index $n^c_{||} = (\frac{Y}{1+Y})^{1/2}$, where $Y = \frac{\omega_{ce}}{\omega}$, two branches of LO-mode and Z-mode waves connect together at the site of the mode conversion where the plasma frequency equals to the wave frequency. In a case that the parallel component of the refractive index of incident waves is slightly different from the critical value of the refractive index, two branches are disconnected and there is an evanescent layer even though the perpendicular component of the refractive index becomes zero for both LO-mode and Z-mode waves. Although the LMCT predicts that the mode conversion does not occur in such a case, the recent simulation results by Kalaee et al. (2009) have shown that the effective mode conversion can be expected under the condition in which the spatial scale of the density gradient is of the order

of the wavelength of the incident UHR-mode waves. Under the initial settings used in Run-3, the parallel component of the refractive index of incident UHR-mode waves is different from the critical value ($n_{||} = 0.3684$ and $n^c_{||} = 0.4682$), and two branches of LO-mode and Z-mode waves are disconnected as show in Fig. 8. We find that all of the wave normal angles assumed in the simulation runs are slightly different from the critical values, as shown in Fig. 8a–c.

The converted LO-mode waves are emitted to the magnetosphere with the corresponding beaming angles. In order to estimate the beaming angle from the simulation results, we first obtained the wave normal angle of LO-mode waves near the region of the mode conversion in Region-A. Using the estimated wave normal angle and assuming Snell's law during the propagation of LO-mode waves toward the region of the lower plasma frequency, we estimate the beaming angle of the LO-mode waves at the region away from the site of the mode conversion. Figure 8a–c shows the variations of the wave normal angle with the constant $n_{||}$ as functions of ω_p/ω_{ce0} under the condition of each simulation run, where ω_{ce0} is the local electron cyclotron frequency at the site of the mode conversion. In each result, the wave normal angle increases during the propagation toward the lower density region and converges an appropriate value corresponding to the propagation angle of LO-mode waves in the magnetosphere. In the result of Run-3, we can obtain the beaming angle α with respect to the magnetic equatorial plane by $\alpha = \left(\frac{\pi}{2} - \theta\right)$, where θ is the wave normal angle of LO-mode waves. As shown in Fig. 8c, we obtained the convergent wave normal angle $\theta \approx 68^\circ$ of LO-mode waves in Run-3, corresponding to the beaming angle $\alpha \approx 22^\circ$. On the other hand, from the observation estimation, plasma frequency ($f_{pe} = 388\,\mathrm{kHz}$) and cyclotron frequency ($f_{ce} = 109\,\mathrm{kHz}$) at the mode conversion point, we obtain $\alpha_{LMCT} = \tan^{-1}\left(\frac{\omega_{ce}}{\omega_{pe}}\right)^{1/2} \approx 27.9^\circ$, which is about 6 degrees larger than the simulation result. We also found differences between simulation results with the LMCT predictions. The differences are 7 degrees and 1 degree respectively corresponding to the results of Run-1 and Run-2, while larger beaming angles are obtained in both results. These results suggest a possibility that the beaming angle of LO-mode waves propagating in the magnetosphere is different from that of the LMCT prediction.

This discrepancy could be explained by the limitation of LMCT which assumes that mode conversion only occurs in the case of the close coupling of plasma waves at the site of mode conversion. Numerical simulation showed that the mode conversion takes place not only in a case that $n_{||} = n^c_{||} =$ constant but also in a case that $n_{||} \neq n^c_{||}$. For the critical value of the wave normal angle, the conversion efficiency is the highest and for other wave normal angles, the conversion efficiency is decreasing as a Gaussian function where the wave normal angle goes far from the critical angle. For the wave normal angles close to critical angle, we expect an effective mode conversion. In our cases the wave normal angles are closed to the critical angle base on the observation.

For comparison between the results of the mode conversion with a critical value of the incident wave normal angle and the results of the mode conversion with other incident wave normal angles, we performed several simulation runs with different propagation angles (30, 55, 60, 75 and 90 degrees; θ=60° is the critical value of the incident wave normal angle) by assuming the same background plasma condition and the same frequency of incident wave as used to event-1. Figure 9 shows the relative wave amplitude profile as a function of wave normal angle of LO-mode wave. The relative wave amplitude in each angle is estimated from the conversion efficiency. Therefore, under the condition that efficient mode conversion is expected, the beaming angle of LO-mode waves could be different with the LMCT prediction

Especially, under the condition that the spatial scale of the density gradient is of the order of the wavelength of incident UHR-mode waves, the efficient mode conversion could be expected and the radio window angle of generated LO-mode waves becomes different from the LMCT prediction (e.g., Kalaee et al., 2009). In the present study we have pointed out that the inhomogeneity with the spatial scale comparable with the wavelength is important in understanding the emission mechanism. However, the detailed processes related to the narrow band nature of the emissions have not been discussed.

The latitudinal beaming angles predicted from the LMCT Jones' theory is not widely supported by the observations (Margan and Gurnett, 1991). Hashimoto et al. (2005) reported the beaming theory is not consistent with the observations since they were observed in wide angles. According to the radio window theory, such a large observed cone angle can only be formed by a series of point sources; Grimald et al. (2007) demonstrated the difficulty of validating NTC linear generation mechanisms using global beaming angle. However, the radio window theory is as yet neither validated nor invalidated. Although we have shown that the efficient mode conversion could be expected in the regions of the observation, we need additional conditions in the generation process so as to explain the narrow band nature of the emissions. Additionally, we assumed the density gradient by referring the observation results but we used the averaged and smoothed inhomogeneity in the simulation system. Since there is a possibility that the fine structure of the density gradient would affect on the efficiencies and propagation angles of converted LO-mode waves, it is important to take into account more realistic density structure in the simulation system. These works are important in the future study.

6 Conclusion

In the present paper, based on the observation results of the Akebono satellite, we studied the properties of the mode conversion processes using two-dimensional electron fluid

simulations. We first analyzed the three observation results of UHR-mode and LO-mode waves by the Akebono satellite around the inhomogeneous region close to the plasmaspause. The wave characteristics of UHR and LO-mode waves were analyzed by comparing the cold plasma dispersion relation, and the spatial inhomogeneity of the background plasma in each event was estimated from the profile of the UHR frequency indicated in the spectrograms observed by PWS instrument onboard the Akebono satellite. For the comparison with the observations, we then performed three numerical experiments corresponding to the three observed events using initial parameters determined from the observation results. The density gradient assumed in the simulation system was determined from the observed f_{UHR}, and the analyzed wave normal angle of UHR-mode waves in each event was used for the wave normal angle of the incident waves in the corresponding simulation run. The simulation results confirmed that the wave energy of the UHR-waves tends to be converted to the LO-mode waves through the mode conversion process, while the wave normal angle and $E_{\mathrm{x}}/E_{\mathrm{y}}$ ratio of generated LO-mode waves were consistent with the observation results.

The results of present study are valid for the computed ratio listed in Table 2.

By analyzing the simulation results, we found a possibility that the radio window (beaming angle) can be different from the prediction of LMCT. Based on the results of the recent simulation studies, the difference of the beaming angle could be explained by considering the condition that the parallel component of the refractive index is slightly different from the critical value in the mode conversion process (Kalaee et al., 2009). The results of present study focus on comparison between simulation and observation thereby suggest the importance of the spatial scale of the inhomogeneity in considering the generation process of LO-mode waves through the mode conversion process in actual space.

Acknowledgements. Computation in the present study was performed by the KDK system of Research Institute for Sustainable Humanosphere (RISH) at Kyoto University and supercomputing resources at Cyberscience Center, Tohoku University as a collaborative research project. This work was supported by Tohoku University Global COE program "Global Education and Research Center for Earth and Planetary Dynamics" and by Grant-in-Aid 22684025 of the Ministry of Education, Science, Sports and Culture of Japan.

Topical Editor R. Nakamura thanks P. Canu and K. Hashimoto for their help in evaluating this paper.

References

Benson, R. F.: Source mechanism for terrestrial kilometric radiation, Geophys. Res. Lett., 2, 52–55, 1975.

Carpenter, D. L. and Anderson, R. R.: An ISEE/Whistler model of equatorial electron density in the magnetosphere, J. Geophysics. Res., 97, 1097–1108, 1992.

Grimald, S., Décréau, P. M. E., Canu, P., Suraud, X., Vallières, X., Darrouzet, F., and Harvey, C. C.: A quantitative test of Jones NTC beaming theory using CLUSTER constellation, Ann. Geophys., 25, 823–831, 2007, http://www.ann-geophys.net/25/823/2007/.

Jones, D.: Source of terrestrial non-thermal radiation, Nature, 260, 686–689, 1976.

Jones, D.: Mode-coupling of Z-mode waves as a source of terrestrial kilometric and Jovian decametric radiations, Astron. Astrophys., 55, 245–252, 1977.

Jones, D.: Latitudinal beaming of plantary radio emissions, Nature, 288, 225–229, 1980.

Jones, D., Calvert, W., Gurnett, D. A., and Huff, R. L.: Observed beaming of terrestrial myriametric radiation, Nature, 328, 391–395, 1987.

Hashimoto, K., Anderson, R. R., Green, J. L., and Matsumoto, H.: Source and propagation characteristics of kilometric continuum observed with multiple satellites, J. Geophys. Res., 110, A09229, doi:10.1029/2004JA010729, 2005.

Hashimoto, K., Green, J. L., Anderson, R. R., and Matsumoto, H.: Review of Kilometric Continuum, in: Lecture Notes in Physics, vol. 687, edited by: LaBelle, J. W. and Treumann, R. A., pp. 37–54, Springer, New York, 2006.

Margan, D. D. and Gurnett, D. A.: The source location and beaming of terrestrial Continuum radiation, J. Geophysics. Res., 96, 9595–9613,1991.

Kalaee, M. J., Ono, T., Katoh, Y., Iizima, M., and Nishimura, Y.: Simulation of mode conversion from UHR-mode wave to LO-mode wave in an inhomogeneous plasma with different wave normal angles, Earth Planets Space, 61, 1243–1254, 2009.

Katoh, Y.: Hybrid simulations of particle acceleration processes due to wave particle interactions, PhD thesis, Tohoku University, Sendai, 2003.

Katoh, Y. and Iizima, M.: A computer simulation study on the mode conversion process from slow X-mode to fast X-mode by the tunneling effect, Earth Planets Space, e53–e56, 2006.

Lembege, B. and Jones, D.: Propagation of Electrostatic Upper-Hybrid Emission and Z Mode Waves at the Geomagnetic Equatorial Plasmapause, J. Geophys. Res., 87(A8), 6187–6201, 1982.

Oya, H.: Conversion of electrostatic plasma waves into electromagnetic waves: numerical calculation of the dispersion relation for all wavelengths, Radio Sci., 12, 1131–1141, 1971.

Oya, H.: Origin of Jovian decametric wave emissions-Conversion from the electron cyclotron plasma wave to the O-mode electromagnetic wave, Planet. Space Sci., 22, 687–708, 1974.

Oya, H., Morioka, A., Kobayashi, K., Iizima, M., Ono, T., Miyaoka, H., Okada, T., and Obara, T.: Plasma wave observation and sounder experiments (PWS) using the Akebono (EXOS-D) satellite-instrumentation and initial results including discovery of the high altitude equatorial plasma a turbulance, J. Geomag. Geoelectr., 42, 411–442, 1990.

Warren, E. S. and Hagg, E. L.: Observation of electrostatic resonances of the ionospheric plasma, Nature, 220, 466–468, 1968.